Wiley
Advances in Civil Engineering
Volume 2024, Article ID 8980592, 10 pages
https://doi.org/10.1155/2024/8980592

WILEY

Research Article

Influence of Mechanical and Microscopic Properties of Red Sandstone Modified by Different Solid Waste Materials

Xiangmei Chen,[1,2] Yongqiang Ren ,[1] Baoli Tang,[1] and Guohui Yang[3]

[1]*Department of Civil Engineering, Ordos Institute of Technology, Ordos 017000, China*
[2]*School of Chemical Engineering, The Inner Mongolia University of Technology, Hohhot 010051, China*
[3]*Baotou City Housing and Urban-Rural Development Bureau, Baotou 014000, China*

Correspondence should be addressed to Yongqiang Ren; ryongqiang@oit.edu.cn

Received 15 February 2024; Revised 26 March 2024; Accepted 22 April 2024; Published 30 May 2024

Academic Editor: Loke Kok Foong

To improve the strength of red sandstone roadbed and elevate the utilization rate of solid waste materials, this study explored the enhancement of red sandstone using three types of solid waste materials: slag-micronized powder, fly ash, and waste incineration bottom ash. The mechanical properties of various solid waste materials, including compaction, unconfined compressive strength, and disintegration test results, were evaluated to assess the enhancement of red sandstone. Additionally, scanning electron microscopy was employed to analyze the microstructural alterations induced by these materials. The results indicated that the optimal moisture content of fly ash-improved soil and slag micropowder-improved soil gradually increased, whereas the maximum dry density decreased with an increase in the solid waste material admixture. At an 11% dosage of waste incineration bottom ash, the maximum unconfined compressive strength reached 2,386 kPa. The soil–water characteristic curves for the different solid waste materials exhibited a similar overall trend. Notably, the disintegration rate significantly slowed at a 9% dosage of fly ash, whereas at 11% dosage of waste incineration bottom ash, the disintegration rate nearly reached 0%, demonstrating optimal improvement effects. This suggested that the bottom ash effectively enhanced the water stability performance of red sandstone and increased its resistance to disintegration. Microscopic analysis revealed that slag micropowder and fly ash were comparatively less effective in enhancing red sandstone. The waste incineration bottom ash efficiently generated substantial cementitious material to fill pores. In summary, employing 11% waste incineration bottom ash was recommended to enhance red sandstone in practical roadbed improvement projects.

1. Introduction

Red sandstone, prone to weathering and disintegration upon contact with water, faces strength degradation due to cyclic dry and wet conditions caused by the Ordos region's high summer rainfall and arid climate. This deterioration adversely affects the stability of the highway structures [1]. The red sandstone in the Ordos region contains a significant proportion of swelling minerals such as illite and montmorillonite. Coupled with soil-forming processes acting on weathered rock debris, this fine-grained clay material tends to accumulate, fostering the formation of agglomerates rich in expansive illite and montmorillonite, thus exhibiting increased expansibility and disintegration potential [2]. Utilizing these weathered rock chips or clay aggregates directly for roadbed filling results in engineering challenges, such as pavement bulging, slurry bubbling, uneven settlement, and inadequate bearing capacity [3]. However, considering the absence of roadbed filler and the imperative to economize on project expenses, local roadbed filling practices are commonly employed. Therefore, investigating the enhancing red sandstone becomes essential.

Currently, the predominant roadbed filler improvers are materials with superior water stability, such as cement and lime, which yield commendable enhancement outcomes [4]. Yanpeng et al. [5] employed cement to solidify red sandstone, yielding significantly improved dynamic soil properties and other metrics after the incorporation of an appropriate cement dosage. Similarly, Shizheng et al. [6] evaluated the impact of fly ash on red sandstone via mechanical and durability tests and observed a decrease in the unconfined compressive strength

with an increase in wet and dry cycles. Although cement and lime can effectively ameliorate the undesirable traits of red sandstone, cement production can cause substantial pollution and the emission of harmful gases, significantly affecting the environment. Additionally, it can alter soil pH, leading to groundwater contamination in the vicinity and affecting local vegetation growth [7]. Lime suffers from drawbacks, such as low water resistance and limited improvement efficacy, failing to address the inherent weathering and disintegration tendencies of red sandstone upon water contact. Furthermore, other chemical curing agents can introduce a certain degree of soil and groundwater pollution [8]. Therefore, the current focal point of research for numerous scholars is the development of methods that exhibit low energy consumption and minimal pollution and are effective in enhancing the mechanical properties of red sandstone materials.

Owing to robust infrastructure growth in China, there has been a significant increase in iron and steel production, leading to an increase in the production of slag micropowder, a solid waste material generated during this process. In line with the principle of "solid waste reuse," Shuai et al. [9] have experimented with incorporating slag micropowder into loess. Their findings indicated that slag micropowder exhibited a degree of activity, thereby effectively enhancing the mechanical properties of the soil. After pretreatment, the domestic waste was directed to the incinerator for disposal. Throughout the incineration process, a significant quantity of solid waste bottom ash is generated from the combustion of waste. Mang et al. [10] have explored the utilization of bottom ash as an aggregate substitute for natural stone in road pavement, sub-base, and roadbed construction. Their findings indicated that bottom ash exhibited a certain level of hydration activity and can enhance the mechanical properties of the roadbed. Fly ash, a solid waste resulting from coal combustion, comprises minerals from the coal residue during the combustion of solid waste materials [11]. Zhangqiong et al. [12] investigated the incorporation of fly ash into clay, observing optimal improvement when the fly ash content was 5%. Primarily, fly ash enhanced red clay through fine particle filling and generation of cementitious substances.

Currently, solid waste materials, such as slag micropowder, fly ash, and waste incineration bottom ash, are underutilized to enhance red sandstone. This study focused on red sandstone in the Ordos area and conducted indoor tests on roadbed soil improvement using solid waste materials: micronized slag powder, fly ash, and bottom ash from garbage incineration. The proportions of the solid waste materials tested were 3%, 5%, 7%, 9%, and 11%. The engineering properties of solid waste materials in improved red sandstone soil in the Ordos area were examined through mechanical and microscopic analyses. The tests included compaction, unconfined compressive strength, disintegration, soil–water characterization, and microscopic electron microscope scanning. The findings can offer insights into enhancing the engineering properties of red sandstone soil in the Ordos area, providing a valuable reference basis for future improvements.

Figure 1: Soil extraction site.

2. Experimental Materials and Methods

2.1. Test Materials

2.1.1. Red Sandstone. This research selected red sandstone in the Kangbashi area of Ordos City. The indoor tests for roadbed soil improvement were conducted, which required both in situ and disturbed soil samples. The in situ samples obtained by ring knife sampling were collected on-site (Figure 1). The basic physical properties of the subgrade soil were determined following the Standard for Geotechnical Test Methods [13, 14], and the test results are detailed in Table 1.

The particle analysis test utilized the sieve method to analyze particles above 0.075 mm. Test sieves with apertures of 10, 5, 2, 1, 0.5, 0.25, 0.1, and 0.075 mm were adopted. Soil samples were obtained using the four-point method to ensure representative specimens. After accurately weighing the specimens retained in each sieve (0.1 g), the sieving process was completed. The test results indicating the percentage of the specimen mass smaller than each particle size are presented in Table 2:

$$x = \frac{m_A}{m_B}, \tag{1}$$

where x represents the mass of the specimen smaller than a certain particle size, expressed as a percentage of the total mass of the specimen (%); m_A represents the mass of the specimen smaller than a certain particle size (g); and m_B represents the total mass of the specimen (g).

2.1.2. Solid Waste Materials. The slag powder utilized in the test was prepared by the Gongyi Longze Water Purification Materials Co. It appeared as a gray powder with a specific surface area of 429 m^3/kg. Its activity index was 84.2% and 98.5% for 7 and 28 days, respectively, and the average particle size was 30 μm. The primary chemical constituents are SiO_2 (31.50%), CaO (34.00%), Al_2O_3 (17.70%), SO_3 (1.64%), Fe_2O_3 (1.03%), and MgO (6.01%).

Fly ash was procured from Shandong Hengwang Group Co. and was characterized by a chemical composition

Table 1: Parameters of the physical properties of red sandstone.

Density (g (cm)^3)	Dry density (g (cm)^3)	Liquid limit	Plastic limit	Proportion	Water content (%)	Plasticity index
1.984	1.7877	25.38	14.36	2.69	10.98	11.02

Table 2: Particle analysis results.

Grain group (mm) percentage content (%)							
>10	10–5	5–2	2–1	1–0.5	0.5–0.25	0.25–0.075	<0.075
3.8755	19.1635	34.0995	6.952	11.0415	5.761	9.2615	9.8455

predominantly consisting of Ca $(OH)_2$ (92%), $CaCO_3$ (4%), and MgO (2%). The waste incineration bottom ash, primarily composed of CaO (43%), Al_2O_3 (7%), SiO_2 (47%), and MgO (5%), shared chemical similarities with volcanic ash, a commonly used mineral admixture in bottom ash materials.

2.2. Test Methods

2.2.1. Sample Preparation. To investigate the optimal water content and maximum dry density of both the improved soil and soil with varying solid waste material proportioning parameters, compaction tests were conducted using an electric compactor. Heavy-duty compaction was performed using a 152 mm diameter and 166 mm height compaction cylinder, based on the particle size composition of the roadbed soil. Compaction specimens 50 mm in diameter and 100 mm in height were prepared. The compaction level was maintained at 90% [15].

2.2.2. Compaction Test. Following the "Standard of Geotechnical Test Methods," compaction tests were conducted on both plain soil and improved soil. The first phase involved uniformly mixing the roadbed soil with 5 kg of dry material. Subsequently, according to the predetermined water content rate, the mixture underwent a 24 hr process of water spraying and smothering to yield an improved wet soil. This soil was then divided into five layers and poured into a compacting cylinder, the surface was leveled, and each layer was compacted. Each layer weighed between 900 and 1,100 g and was subjected to 56 blows per layer. Furthermore, shaving is required at the intersection surface of the two layers [16]. The height of the specimen above the top of the compaction cylinder was maintained at less than 6 mm upon the completion of compaction.

2.2.3. Disintegration Test. To further examine the disintegration characteristics of both the plain and improved soils, the specimens were subjected to a disintegration test using a disintegrometer. To mitigate the impact of specimen size and shape on the test results, uniform ring knife samples, each with a size of 200 cm^2 (area), were utilized. The specimen was positioned centrally within the disintegrometer stencil. Upon starting the stopwatch, it was rapidly introduced into the water cylinder while holding the float tube. Readings of the float cylinder were immediately taken at the onset, with subsequent readings recorded every 10 s during the test to assess the disintegration progress. Adjustments to the time interval between readings were made based on disintegration rate.

Figure 2: Disintegration experiment.

2.2.4. Unconfined Compressive Strength Tests and Soil–Water Characteristic Curves. The unconfined compressive strength test was performed using a YSH-2 unconfined pressure meter. To assess the soil–water characteristics of both plain and improved soils, specimens were prepared, pumped, and saturated. Subsequently, the soil–water characteristic curves were determined using the GEO Expert pressure plate instrument. A specific air pressure was applied throughout the test. Upon cessation of drainage, the pressure was released, and the specimen mass was measured before proceeding to the next pressure level. After completion of the test, the specimens were dried, and their dry masses were measured to calculate the water content at each pressure level and construct the soil–water characteristic curve.

2.2.5. Disintegration Test. To analyze the disintegration characteristics of both plain and improved soils, a disintegrometer was employed following the relevant industry standards (Figure 2). The specimen was positioned at the center of the stencil, and upon starting the stopwatch, it was immediately immersed in the water cylinder while holding the float. The initial readings of the float cylinder were taken along with the start time. Subsequently, readings were recorded every 10 s during the test to evaluate the disintegration progress by adjusting the time interval based on the rate of disintegration. Upon completion, the disintegration rate of the specimen was calculated, and a disintegration curve was plotted with the disintegration rate as the vertical coordinate and disintegration time as the horizontal coordinate.

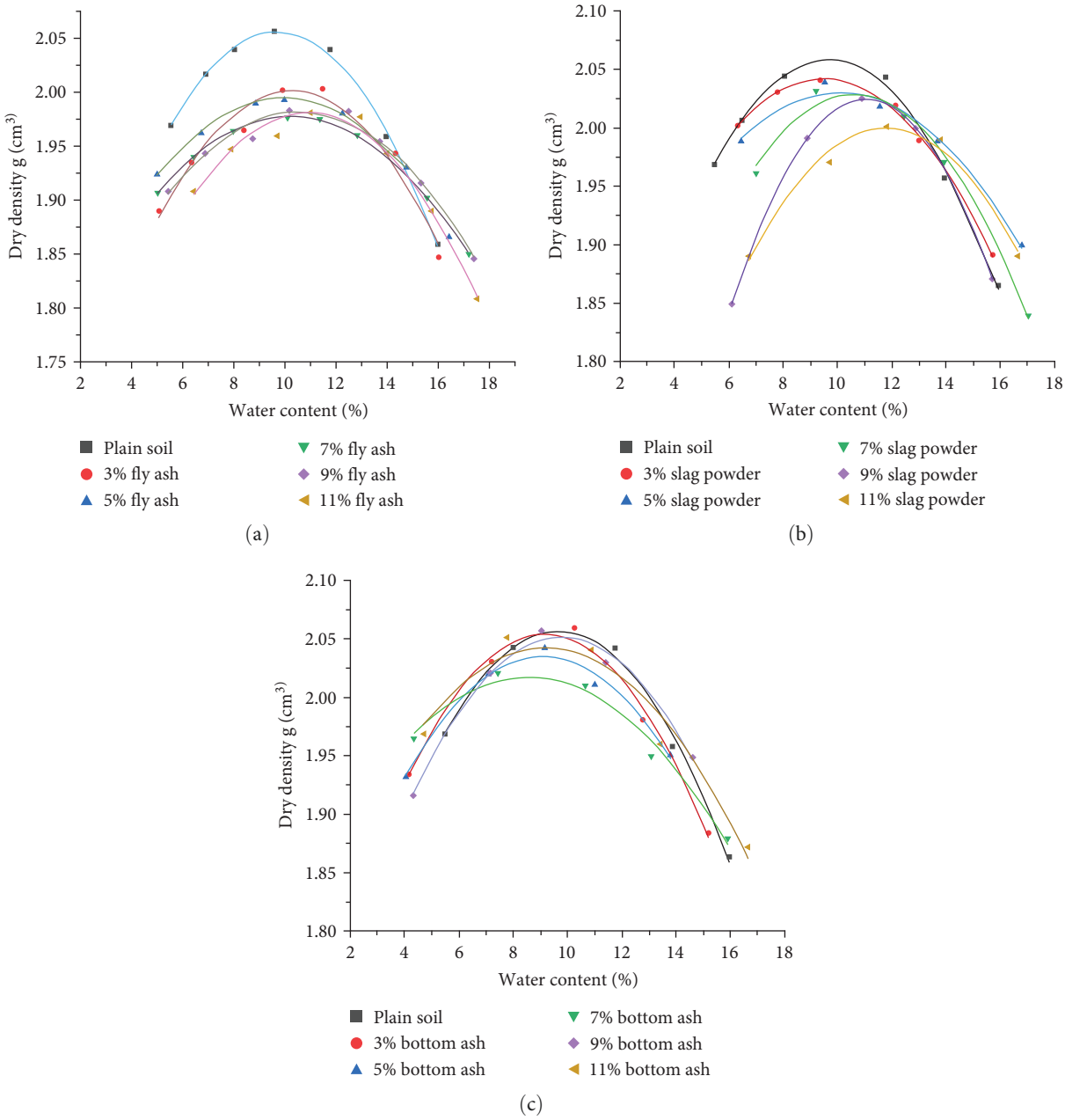

Figure 3: Compaction curves of modified soil. (a) Fly ash-amended soil compaction curves. (b) Compaction curve of slag powder-amended soil. (c) Compaction curves for improved soils with bottom ash from waste incineration.

2.2.6. Microscopic Testing. The microscopic tests were conducted using an environmental scanning electron microscope (ESEM) manufactured by FEI, Ltd. The ESEM scanning electron microscope can offer high resolution, a long depth of field, and stereoscopic imaging, rendering it extensively utilized in geosciences. First, a low magnification was employed to roughly select the area of interest, followed by zooming in for detailed observation. The sample stage orientation was adjustable, enabling a rotation of 360°, tilting from 0° to 90°, and panning across three spatial dimensions. The scanning capabilities included a 100 mm pan along the X- and Y-axes and 50 mm of elevation along the Z-axis.

3. Results and Discussion

3.1. Compaction Test. Based on the compaction test data for the improved soil with fly ash, slag-micronized powder, and waste incineration bottom ash, compaction curves were constructed for both plain soil and improved soil specimens. These curves plot the dry density on the horizontal axis and water content on the vertical axis. The peak point on the curve represents the maximum dry density and optimum water content of the soil, with vertical and horizontal coordinates indicating these values, respectively. Figure 3 illustrates the compaction curves.

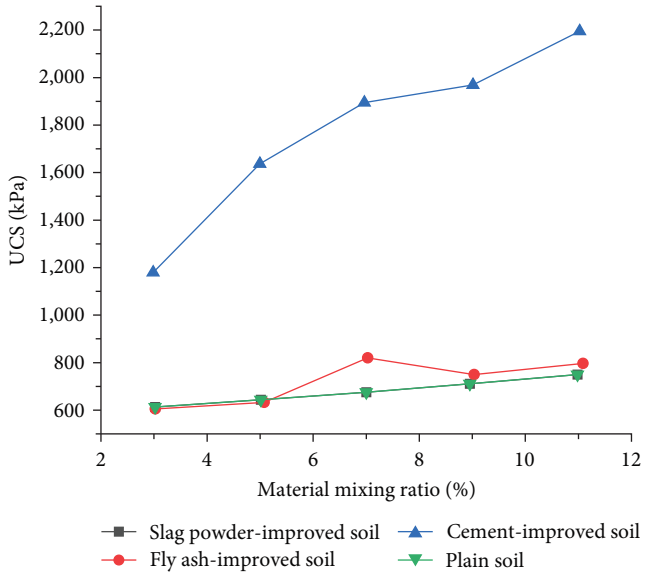

FIGURE 4: Variation of unconfined compressive strength of modified soil.

From the figure, the maximum dry densities of fly ash-improved soil, slag-micronized soil, and waste incineration bottom ash-improved soil were 2.055 g/cm^3, 2.055 g/cm^3, and 2.06 g/cm^3, respectively. Examining the compaction curves suggested that the optimum moisture content of fly ash-improved soil and slag-micronized soil-improved soil gradually increased with the incorporation of solid waste materials, contributing to a gradual decrease in the maximum dry density. This can be primarily due to the hydration reactions between fly ash, slag-micronized powder, and water, which required increased water content for soil compaction. Simultaneously with the cohesion and flocculation of soil particles, larger particles of improved soil form, decreasing the soil compaction effect and resulting in a decreased dry density. The optimal water content and the maximum dry density of the soil improved by waste incineration bottom ash and decreased with increasing bottom ash dosage. When the bottom ash mixing amount was 7%, the maximum dry density of the specimen reached a minimum of 2.029 g/cm^3, representing a 5.75% reduction compared to the vegetal red sandstone soil. At 11% fly ash-improved soil dosing, the optimum water content was 11.8%, a 4.67% increase over the plain red sandstone soil. Similarly, with an 11% dosage of slag-micronized modified soil, the optimal water content was 12.0%, indicating a 5.43% increase over plain red sandstone soil.

3.2. Unconfined Compressive Strength Test. The unconfined compressive strength curves of the modified red sandstone with various solid waste materials are shown in Figure 4. It can be evident that the unconfined compressive strength of plain red sandstone was 523 kPa, which failed to meet the engineering strength criteria. The enhanced red sandstone, incorporating three different solid waste materials, exhibited a notably greater increase in unconfined compressive strength than plain red sandstone. Moreover, this strength enhancement demonstrated a nearly linear relationship with the proportion of solid waste material. Among these enhancements, the unconfined compressive strength of the improved soil reached its maximum of 563 kPa when the fly ash incorporation ratio was 7%. Similarly, the unconfined compressive strength of the waste incineration subsoil increased with the augmentation of subsoil ash incorporation, presenting a significant improvement. Specifically, at an 11% proportion of bottom ash, the maximum unconfined compressive strength was 2,386 kPa, representing a 76.41% increase over plain red sandstone. This enhancement was primarily attributed to the relatively high CaO content (37%) in the bottom ash, which facilitated the generation of cementitious substances and the formation of a stable and impermeable protective film around the soil particles. This enhanced soil compactness. Conversely, slag powder, with its low CaO (34%) and SiO_2 (31.50%) contents, inhibited the formation of cementitious substances, thereby affecting the late-stage strength of the soil. In summary, the highest unconfined compressive strength was observed in waste incineration bottom ash-improved soil, while the enhancements in unconfined strength for fly ash-improved soil and slag-micronized improved soil were comparable, albeit lower than those of waste incineration bottom ash-improved soil.

3.3. Changes in Soil–Water Characteristic Curves. Figure 5 illustrates the variation in the soil–water characteristic curves of the red sandstone-amended with various solid waste materials. The larger the dosage, the greater the residual water content of the specimen and the stronger its water-holding characteristics under equivalent matrix suction. At suction forces exceeding 60 kPa, the soil–water curve of waste incineration bottom ash-improved soil tended to flatten, and the changes in water content with increasing matrix suction were small, which was close to the residual water content. Moreover, with increasing dosage, the specimen exhibited enhanced water-holding capacity and improved water stability. Owing to the compression of internal large pores by bottom ash improvement, accompanied by the effective filling of these pores with gelling material generated by bottom ash, the resulting soil exhibits improved water-holding capacity. Moreover, the medium pores were relatively widely distributed, which further contributed to the capacity. The slopes of the soil water curves for slag powder improvement were smaller than those of the untreated soil, indicating a stronger water-holding capacity and enhanced water stability. Similarly, fly ash improvement also enhances water stability compared to untreated soil, with the water-holding capacity becoming increasingly evident with dosage increments. Figure 4 illustrates a consistent trend in the soil–water characteristic curves of various solid waste materials, which were generally divided into two segments. Between 0 and 60 kPa suction force, the curve slope decreased notably, indicating the opening of most gas channels in the pores, facilitating air penetration into the soil. As the suction force increased, the free water in the pores was rapidly expelled, leading to a rapid decrease in the soil body saturation. In the range of 60–500 kPa suction force, the curve slope became gentler, marking the boundary effect zone. The saturation was higher,

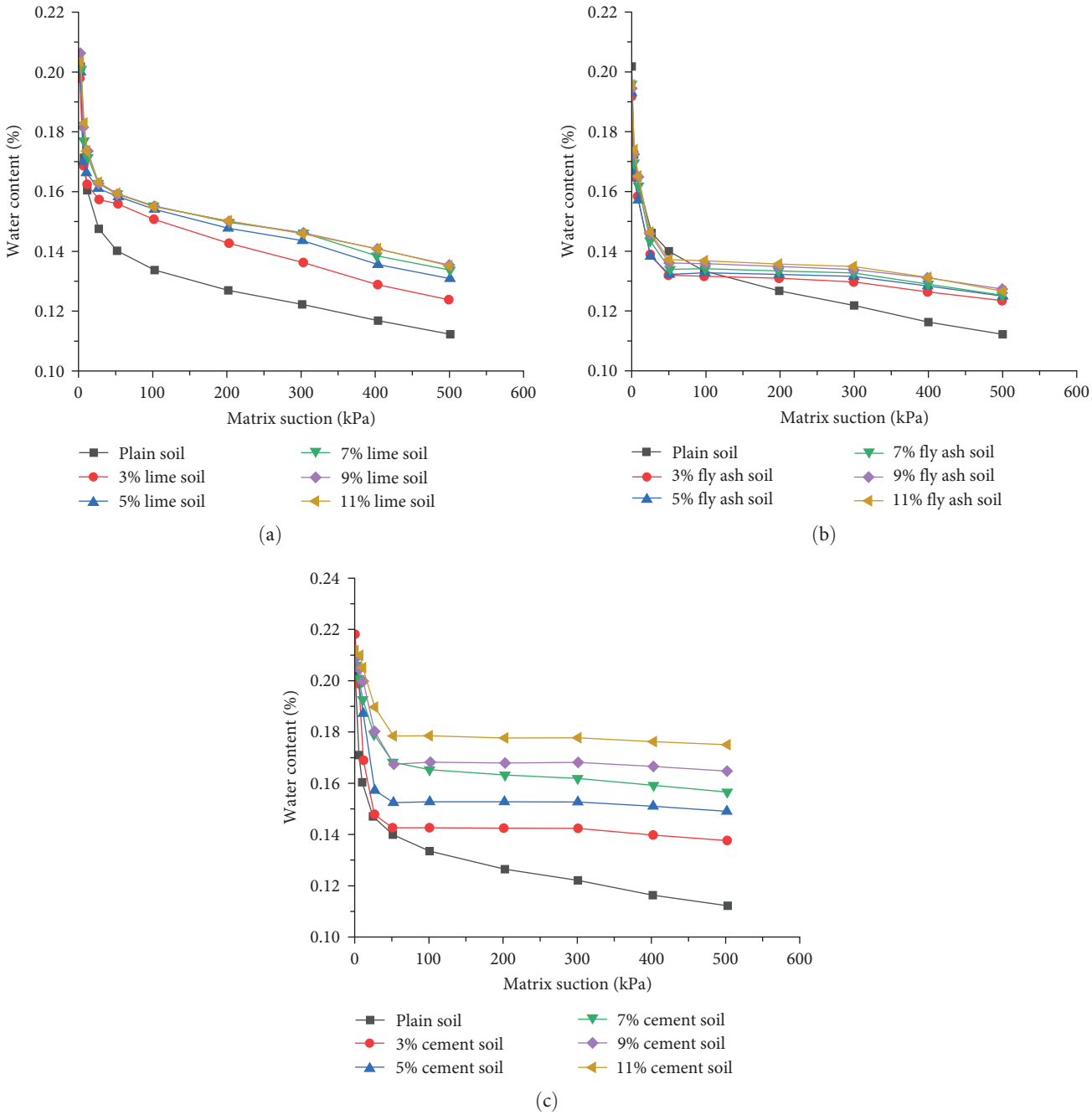

Figure 5: Characteristic curves of soil water in modified soil. (a) Soil–water characteristic curves for fly ash-amended soils. (b) Characteristic curves of soil–water characteristics of slag-micronized amended soil. (c) Characteristic curves of soil and water characteristics of soil amended with bottom ash from waste incineration.

gas within the pore space was in a closed state, and water expulsion from the pore space was hindered.

3.4. Disintegration Test. Figure 6 illustrates the disintegration rate of the red sandstone modified with various solid waste materials over time. The disintegration rate notably increased within 150 s of the addition of fly ash. This acceleration primarily resulted from immediate disintegration upon immersion in water, leading to gravitational imbalances among the particles and rapid air expulsion from the soil. Simultaneously, increased air pressure can result in particle extrusion, causing the surface layer particles to peel off until the specimen disintegration rate reached 100%. This indicated that the fly ash-amended red sandstone still lacked effective enhancement of interparticle cementation [17]. The disintegration notably decelerated at a 9% dosage of fly ash, reaching its lowest rate (16%) at 11%. As the amount of micronized slag powder doping increased, the disintegration curve progressively decelerated. However, even at a doping level of 11%, the disintegration rate of the red sandstone remained 100%

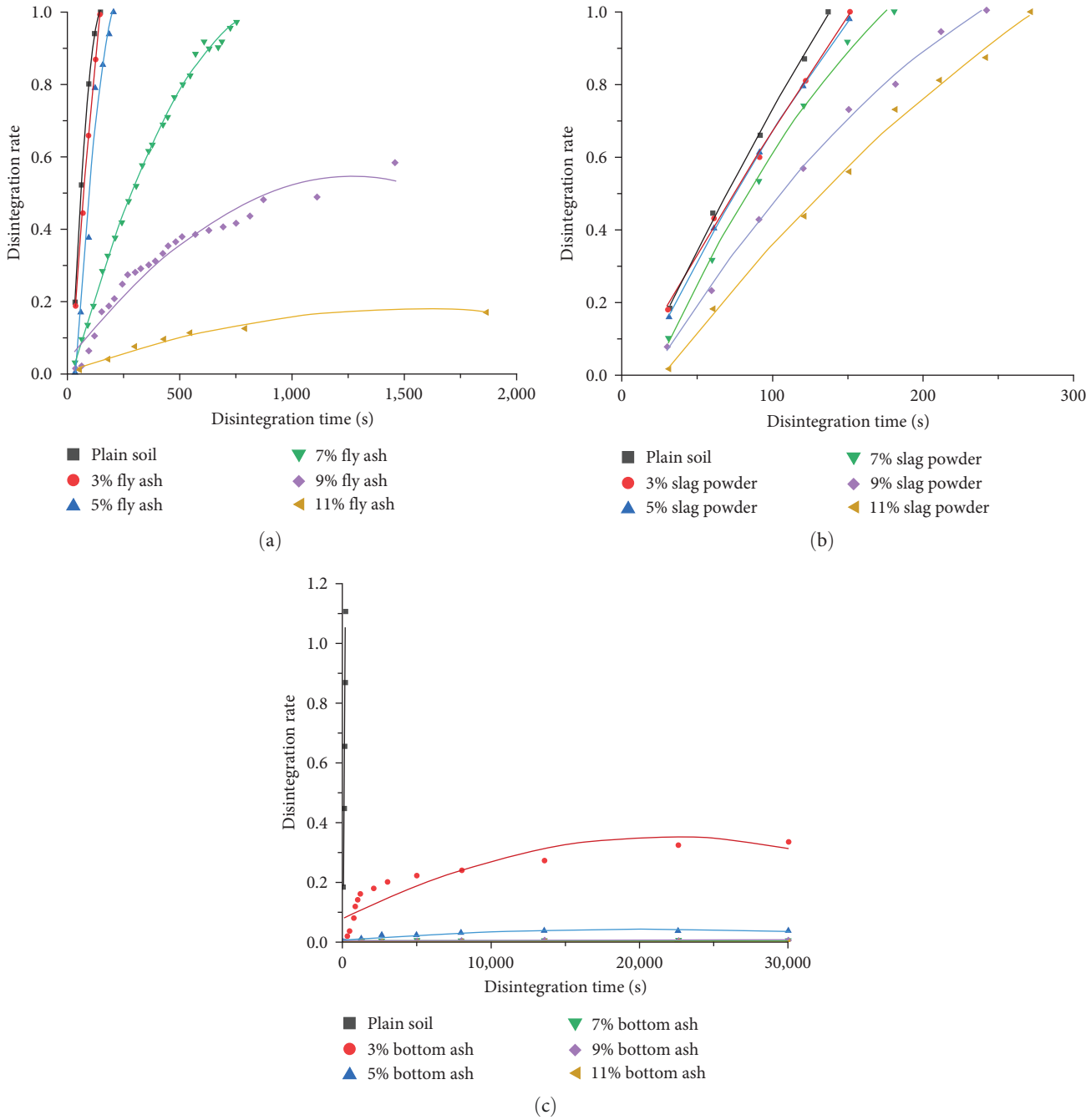

Figure 6: Disintegration curves of red sandstone modified by different solid waste materials. (a) Disintegration curves of fly ash-amended soils. (b) Disintegration curves of slag powder-micronized amended soil. (c) Disintegration curves for waste incineration bottom ash-amended soils.

within 270 s. This suggested that the micronized slag powder cannot effectively enhance the resistance of red sandstone to disintegration. The disintegration curves in Figure 6(c) illustrate that the disintegration rate of the bottom ash-modified soil specimens decreased as the bottom ash doping increased. Notably, the specimens doped with 3%–11% exhibited minimal disintegration, indicating weak susceptibility. At an 11% dosage, the disintegration rate was 0%, demonstrating the substantial enhancement of water stability and disintegration resistance in red sandstone. This suggested that the bottom ash effectively prolonged the stabilization period of the residual soil in contact with water. Furthermore, the antidisintegration effect on red sandstone was optimized at an 11% dosage. The primary reason for this can be that before the improvement of red sandstone with waste incineration bottom ash, the particles primarily featured point-based contact and the contact areas and significant pore space between particles. When exposed to a water load, the soil structure deteriorated, and the particles were prone to substantial particle displacement, ultimately reducing the stability of the soil

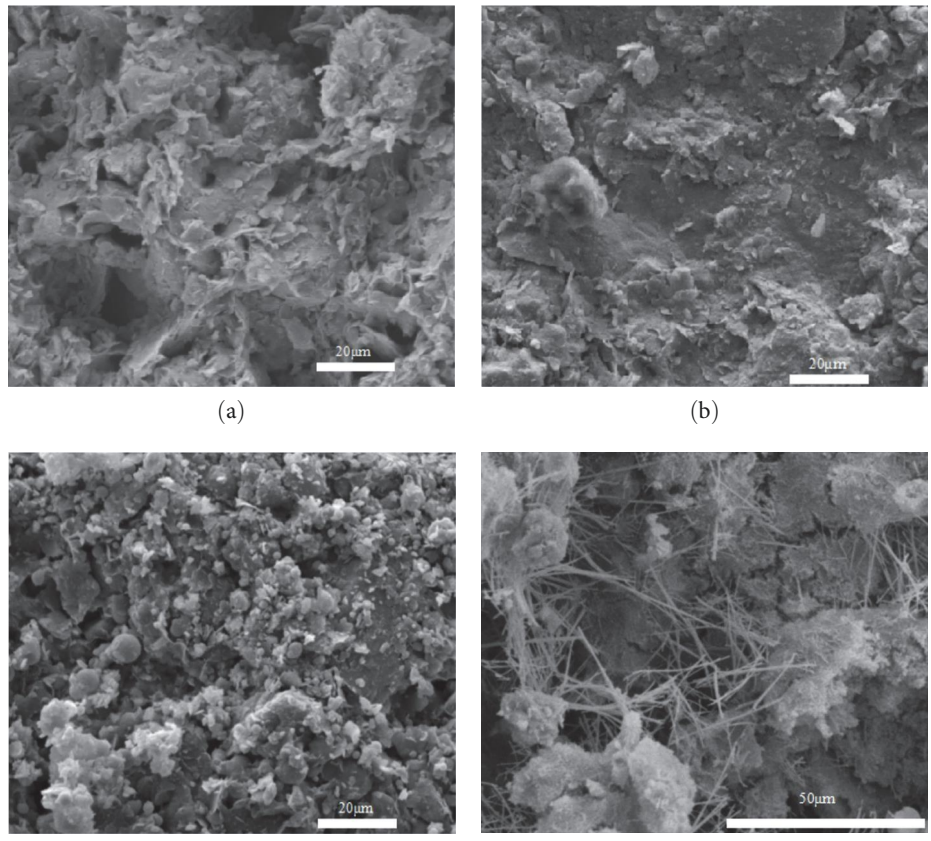

Figure 7: SEM images. (a) Vegetative soil microstructure (b) Microstructure of fly ash-amended soils. (c) Microstructure of slag-micronized amended soils. (d). Microstructure of waste incineration bottom ash-amended soils.

body. However, upon mixing waste incineration bottom ash into the soil, the soil skeleton transitioned gradually from red sandstone particles to those supported by waste incineration bottom ash. Under the influence of water load, smaller-diameter loess particles can fill the gaps between the waste incineration bottom ash particles, and both the pore area and diameter were reduced. Simultaneously, the contact area between the red sandstone particles and bottom ash expanded, augmenting friction and enhancing the pore structure, thus improving the strength of the soil skeleton. Furthermore, the higher CaO content (43%) in waste incineration bottom ash than slag micropowder and fly ash was significant. Upon contact with water, CaO reacts to form $CaCO_3$, which further filled the pores, consequently promoting the water stability and resistance to disintegration.

3.5. Microimprovement Mechanism of Red Sandstone Improved by Solid Waste Materials. Ultrahigh-pressure electron scanning (UHPES) was conducted on both untreated and treated soil specimens using an electron microscope to investigate the microscopic improvement mechanism of the enhanced soil. Figures 7(a), 7(b), 7(c), and 7(d) displays SEM images magnified to 1,200 times. These images clearly illustrate the enhanced effect of each solid waste material on the treated soil. In Figure 7(a), the soil particles exhibited a flaky morphology with a loose structure and sizable pores, which was characteristic of vegetal soil. Figure 7(b) reveals the soil particles in the fly ash-enhanced soil, characterized by a flaky morphology, whereas the enhancement was evident as the soil structure densified and pore space decreased significantly. The improvement mechanism of the fly ash-enhanced soil encompassed ion exchange, flocculation, carbonation, and cementation effects. Primarily, it involved the reaction between CaO and MgO within fly ash and soil particles, exchange of decomposed Ca^{2+} and Mg^{2+} with Na^{+} and K^{+} ions, or the carbonization of soil particles through reaction with atmospheric CO_2 [18]. In Figure 7(c), the distinct flakiness of soil particles in the slag-micronized amended soil was less prominent, and the pronounced presence of gelatinous spherical junctions of slag-micronized powder was evident. This phenomenon arose because of the high content of active silicon and aluminum in the slag micronutrient powder, which facilitated the formation of stable hydrated calcium silicate and hydrated calcium aluminate, akin to microbeads. This enhanced the ease of mixing and promoted soil particle compaction. The improvement effect of slag micropowder primarily involved ion exchange, flocculation, and hard coagulation reactions to improve the soil strength. In

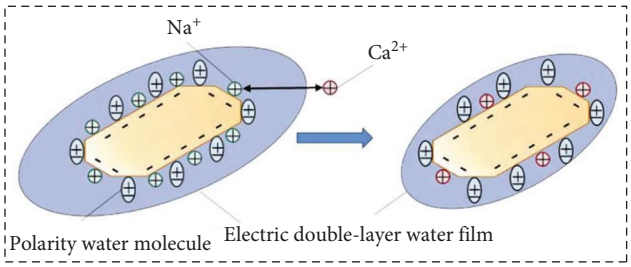

FIGURE 8: Ion exchange action.

Figure 7(d), the soil particles in the bottom ash-enhanced soil no longer exhibited a flaky morphology. Conversely, cementation caused particle agglomeration, with noticeable growth of calcium alumina between the pores. This transformation primarily resulted from the hydration reaction and cementation facilitated by the bottom ash enhancement, leading to the formation of carbonate and aluminum water compounds, dehydration, and crystallization, consequently altering the nature of the soil. The proliferation of needle-like calcium alumina within the soil pores significantly enhanced water stability and soil strength. In summary, the microstructural enhancement effect of waste incineration bottom ash-enhanced soil was superior, providing further insight into the underlying rationale for its heightened mechanical properties.

Furthermore, because waste incineration bottom ash can comprise electrolyte materials, ionized divalent cations (Ca^{2+} and Mg^{2+}) can readily replace monovalent cations (K^{+} and Na^{+}) adsorbed on the surface of minerals such as montmorillonite and other red sandstone particles. This displacement disrupted the bilayer structure on the surfaces of the red sandstone particles. The release of weakly bound water from the outer electric layer contributed to the thinning of the water film in that layer, as depicted in Figure 8. Concurrently, ion exchange elevated the cation valence, reducing the repulsion between particles and further thinning the double electric layer water film. This process led to flocculation, which enhanced the binding force between soil particles, thus forming a stable agglomerate structure and achieving effective soil amelioration.

4. Conclusion

This study examined the utilization of three solid waste materials, including slag micropowder, fly ash, and waste incineration bottom ash, to enhance red sandstone. Various mechanical properties, including compaction, unconfined compressive strength, disintegration, and scanning electron microscopy, were evaluated. The unconfined compressive strength of red sandstone improved with each of the three solid waste materials and showed a greater increase than that of the plain red sandstone. The unconfined compressive strength of red sandstone improved with all three types of solid waste materials and presented a greater increase than the plain red sandstone. Additionally, the strength exhibited a nearly linear growth with an increase in the mixing ratio of the solid waste materials. The highest unconfined compressive strength was observed in soil with waste incineration bottom ash. Moreover, the increase in the unconfined strength of the soils improved with fly ash and slag micropowder was similar, albeit smaller than that of the soils improved with waste incineration bottom ash. The disintegration rate of the red sandstone remained at 100% within 270 s at an 11% dosage of the slag micronizer. Future efforts to enhance soil using waste incineration bottom ash should focus on the microscopic properties and chemical reactions of the soil. Furthermore, combining waste incineration bottom ash with chemical reinforcing agents can improve the soil quality. In roadbed construction, it is essential to intensify the monitoring of waste incineration bottom ash roadbed settlement while increasing roadbed crushing operations.

Data Availability

The datasets used and/or analysed during the current study available from the corresponding author on reasonable request.

Conflicts of Interest

The authors declare that they have no conflicts of interest.

Authors' Contributions

Xiangmei Chen initiated the study; Baoli Tang and Guohui Yang designed the scope of study; Xiangmei Chen analyzed data and wrote the manuscript; Yongqiang Ren reviewed the manuscript.

Acknowledgments

This work was supported by the Inner Mongolia Natural Science Foundation (Grant No. 2020MS04006), scientific research project of Ordos Institute of Technology (Grant No. KYZD2019002), scientific research project of Academician and expert workstation of mine geology and environment, Ordos Institute of Technology (Grant No. 2021 OITYSZJGZZ-008), Ordos mining area geological disaster prevention and geological environmental protection engineering research center, the key project of natural science and technology of Ordos Institute of Technology (Grant No. KYZD2023004), scientific research project of Academician and expert workstation of mine geology and environment, Ordos Institute of Technology (Grant No. 2023 OITYSZJGZZ-004).

References

[1] L. Jiayi, C. Longxu, and Z. Jingrong, "Experimental study on shear strength characteristics of red sandstone improved soil under dry wet cycles," *Highway*, vol. 67, no. 10, pp. 331–342, 2022.

[2] C. Jun, "Study on the mechanical properties and micro mechanism of alkali slag gypsum cement combined solidification of fly ash," *Comprehensive Utilization of Fly Ash*, vol. 38, no. 4, pp. 98–105, 2022.

[3] S. Hepeng and L. Wenbao, "Research on the mechanical properties of red sandstone filling material and its roadbed filling technology under dry wet cycling," *China Science and Technology Information*, vol. 18, pp. 88-89, 2021.

[4] C. Longxu, W. Shuai, L. Datian, and Z. Jingrong, "Study on the control of resilience modulus of red sandstone roadbed filler under dry wet cycling," *Zhongguo Highway*, vol. 40, no. 4, pp. 250–255, 2020.
[5] Y.-P. Zhu, T. Ma, X.-H. Yang, K.-B. Yang, and H.-M. Wang, "Shear strength test and regression analysis of red sandstone improved soil based on orthogonal design," *Journal of Geotechnical Engineering*, vol. 40, no. S1, pp. 87–92, 2018.
[6] F. Shizheng, Y. Renshu, L. Yongliang, and Y. Yang, "Experimental study on dynamic fracture characteristics of frozen red sandstone based on NSCB method," *Journal of Engineering Science*, vol. 45, no. 10, pp. 1704–1715, 2023.
[7] Z. Zhe, C. Shanxiong, D. Zhangjun, H. Kang, and Y. Fei, "Study on the strength softening law of cenozoic red sandstone based on point load test," *Geotechnical Mechanics*, vol. 42, no. 11, pp. 2997–3007, 2021.
[8] X. Lanfu and H. Xiangshui, "Research on the application of intelligent compaction construction technology for red sandstone soil roadbed," *Science and Technology Innovation and Application*, vol. 13, no. 23, pp. 189–192, 2023.
[9] W. Shuai, Z. Jingrong, R. Lei, Y. Yaqin, and C. Longxu, "Experimental study on improvement of red sandstone roadbed filler for huaizhi expressway," *Roadbed Engineering*, no. 6, pp. 145–149, 2018.
[10] Y. Meng, L. Qun, B. Liang, and M. Yingjun, "Experimental study on the influencing factors of unconfined compressive strength of red sandstone improved soil," *Journal of Qingdao University of Science and Technology (Natural Science Edition)*, vol. 38, no. S1, pp. 161–164, 2017.
[11] H. Jian and R. Bo, "The application of mixed ash improvement in the construction of red sandstone roadbed filling," *Sichuan Building Materials*, vol. 45, no. 6, pp. 158-159, 2019.
[12] W. Zhangqiong, G. Yun, L. Shen, and Y. Guohui, "Experimental study on the engineering properties of fly ash modified red sandstone residual soil," *Journal of Engineering Geology*, vol. 26, no. 2, pp. 416–421, 2018.
[13] L. Yuanlian, "Experimental study on water stability of cement modified red sandstone filler," *Hunan Transportation Technology*, vol. 46, no. 4, pp. 23–26+44, 2020.
[14] G. Huifang, W. Wenjun, M. Su, and N. Yuxing, "Effects of different solidification materials and content on the engineering properties of red sandstone," *Highway Transportation Technology (Applied Technology Edition)*, vol. 13, no. 1, pp. 59–61, 2017.
[15] W. Zhangqiong, B. Junlong, and Y. Zhangyan, "Macroscopic experimental study on the mechanism of the "negative effect" of excessive fly ash on fine-grained soil improvement," *Journal of Wuhan Engineering University*, vol. 42, no. 3, pp. 316–320, 2020.
[16] L. Haiying, L. Guilin, and Z. Wen, "Feasibility analysis of directly filling the roadbed under highways with red sandstone," *Anhui Architecture*, vol. 29, no. 8, pp. 129-130 +176, 2022.
[17] Z. Weijun, W. Yongsheng, and M. Tao, "Experimental study on compressive modulus of red layered soft rock improved soil based on orthogonal design," *Journal of Seismic Engineering*, vol. 44, no. 2, pp. 264–269, 2022.
[18] W. Haiming, Z. Yanpeng, D. Zhu, and X. Zenghong, "Experimental study on permeability and physical and mechanical properties of special red sandstone in Lanzhou region," *Gansu Science and Technology*, vol. 35, no. 6, pp. 20–23, 2019.